Author's final manuscript
Published as:
Nucl. Fusion 59, 016016, 2019
https://doi.org/10.1088/1741-4326/aaef0c

dfkong@ipp.ac.cn, xu2@llnl.gov

$E \times B$ flow shear mitigates ballooning-driven ELMs at high collisionality: Experiment and Simulation

D.F. Kong*,[1,2] X.Q. Xu*,[2] P. H. Diamond,[3] J.G. Chen,[4] C. B. Huang,[1] T. Lan,[5] X. Gao,[1] J.G. Li,[1] and EAST Team[1]

[1]*Institute of Plasma Physics, Chinese Academy of Sciences, Hefei 230031, China.*

[2]*Lawrence Livermore National Laboratory 7000 East Avenue, Livermore, 94550, CA, USA*

[3]*Center for Astrophysics and Space Sciences and Department of Physics, University of California San Diego, La Jolla, CA 92093-0429, USA*

[4]*Fusion Simulation Center and State Key Laboratory of Nuclear Physics and Technology, School of Physics, Peking University, Beijing 100871, China.*

[5]*Department of Modern Physics, University of Science and Technology of China, Hefei 230026, People's Republic of China.*

(Dated: October 18, 2018)

By using the specific co-NBI and ctr-NBI systems on EAST, an alternating $E \times B$ flow shear discharge has been performed to study the impact of the $E \times B$ flow shear on ballooning-driven ELM at a fixed high collisionallity ($\nu^* \sim 2.3$). The results reveal that the increased $E \times B$ flow shear can significantly mitigate the ELM, or even totally suppress the ELM when the shear is large enough. Our simulations with BOUT++ support the observations on EAST, and further indicates that the increased $E \times B$ can both reduce the linear growth rate of ballooning mode and shorten its growth time (phase coherence time, PCT) . The enhanced nonlinear interactions shorten the PCT of ballooning mode, which is validated by the bispectrum study on EAST. All those studies suggest a new way to control the ELM.

PACS numbers:

To minimize the size, thus the costs of the fusion devices, a high confinement operation (H-mode), which is characterized an edge transport barrier or pedestal, has been chosen as the baseline scenario of ITER. H-mode typically exhibits fast, quasi-periodic relaxation bursts called edge localized modes (ELMs) on a fast Magnetohydrodynamics (MHD) timescale, that eject particles and energy from the plasma edge. Large type-I ELMs typically lead to large energy fluxes to the plasma facing components (PFCs), which then suffer from excessive ablation, fast erosion, or melting. Thus the mitigation of type-I ELMs for future tokamaks like ITER becomes an important issue for our study. Solar flares are the stellar equivalent of edge localized modes and can be greatly affected by the magnetic shear[1, 2]. Our study focusses on the impact of the flow shear (exhibiting similar effect in turbulence scale) on ELM.

The theoretical works predict that $E \times B$ shear can affect the magnitude and evolution of the cross phase of the velocity $\tilde{v}$ and pressure $\tilde{P}$ fluctuations in the peeling-ballooning-mode-driven heat flux. In one instance, this causes the evolution from ELMing H-mode to quiescent (Q) H mode [3–6]. Experimental results on DIII-D report that the increased $E \times B$ velocity shear can also help to excite the edge harmonic oscillations (EHO), which replaces ELMs and provides reduced continuous heat flux to divertor plates. In addition, a systematic study of the effects of counter (ctr) plasma rotation on ELM characteristics has been performed using a combination of tangential and perpendicular neutral beam injections (NBIs) in JT-60U [7–10]. ELM characteristics (e.g. amplitude, frequency and type) change from those of type-I ELMs to high frequency grassy ELMs (high plasma triangularity) or QH-mode (low plasma triangularity) as counter plasma rotation is increased[7]. With the nonlinear reduced MHD code JOREK, the influence of poloidal equilibrium rotation in MHD simulations of edge-localized modes has been also been studied[11, 12].

On EAST, the experiments are usually carried out at the high collisionality regime with typical parameters, $B_T = 1.57T$, $I_p = 450kA$ and line averaged density $n_e = 2.8 \times 10^{19} m^{-3}$, as illustrated by the black solid curve in Figure 1 (b). The density is kept constant by the density feedback with SMBI (Supersonic molecular beam injection), as shown in Figure 1 (c). The H-mode plasmas are achieved in a low-recycling regime due to extensive lithium wall coating, with the combined lower hybrid wave (LHW) and ion cyclotron resonant frequency (ICRF) hydrogen minority heating, at a power of $P_{LHW,4.6GHz} = 1.5MW$, $P_{LHW,2.45GHz} = 0.5MW$. Deposition of ICRF is at the center of deuterium plasmas. After the L-H mode

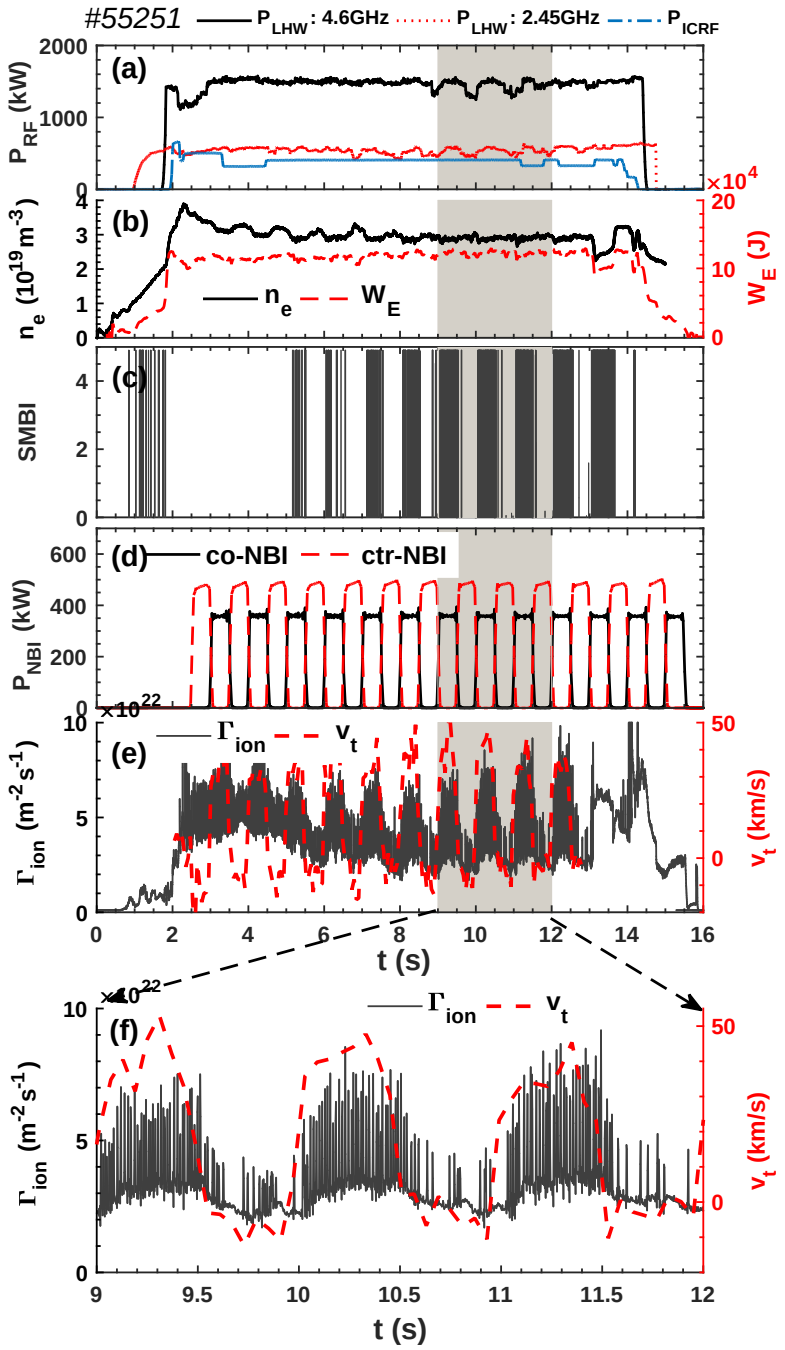

FIG. 1: Time histories of various plasma quantities for a H- mode plasma discharge #55251 on EAST during the application of periodically alternating neutral beam injection. (a) LHW power P_{LHW} ($2.45GHz$ and $4.6GHz$) and ICRF power P_{ICRF}, (b) line averaged density n_e and stored energy W_E, (c) pulse signal of Supersonic molecular beam injection (SMBI), (d) co- and counter-current NBI power P_{NBI}, (e) (f) the density of particle flux Γ_{ion} at the divertor target (black solid line) and the velocity of toroidal rotation of the central plasma v_t (red dash line).

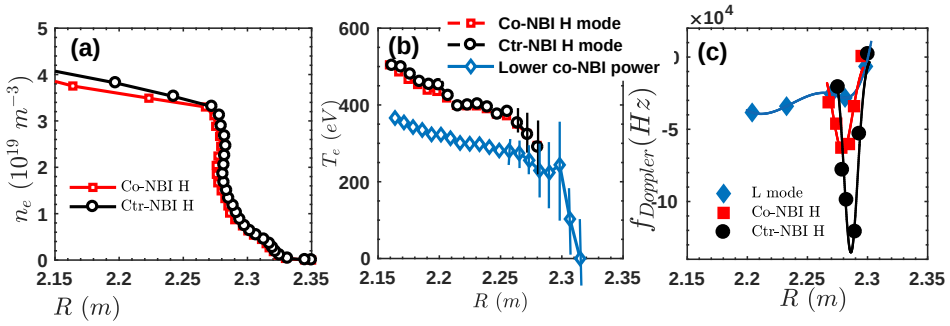

FIG. 2: Radial profiles of (a) electron density n_e, (b) temperature T_e and Doppler shift $f_{Doppler}$(here, $E_r \propto f_{Doppler}$) with co- and counter-current NBI in H-mode discharge, respectively. The blue line is profiles in L-mode discharge.

transition, the H-mode plasma are modulated by periodically alternating the direction of Neutral Beam Injection (NBI), either co-NBI or ctr-NBI (counter-NBI) with $P_{co-NBI} = 0.4MW$ and $P_{ctr-NBI} = 0.5MW$, respectively, as shown in Figure 1 (d). The launch angles of the co-NBI and ctr-NBI are 19.5 and 17, respectively. Those two values are close to each other. With the alternating of the co-NBI and ctr-NBI, the velocity of the toroidal rotation in plasma centre is changed periodically from $\sim 50km/s$ (co-NBI) to $\sim -10km/s$ (ctr-NBI), as illustrated as the red-dash line in Figure 1 (e) and (f).

We have also estimated the divertor particle flux at the strike point with $\Gamma_{ion} = nc_s \sim I_s/eA_s = 2 \sim 7 \times 10^{22} m^{-2}s^{-1}$, where n and c_s are the electron density and ion sound speed at the target, respectively, as shown in Figure 1 (e). Those evolutions indicate that both the size and frequency of ELMs are modulated by the periodically change of NBI. With $0.4MW$ co-NBI, the size of ELM is large and frequency of ELM burst $f_{ELM} \sim 80Hz$ is high. However, for $0.5MW$ ctr-NBI case, the ELM size is suppressed significantly and frequency of ELM reduced to $f_{ELM} \sim 35Hz$. Thus the total particle flux contributed by the ELM is reduced by $70\% \sim 95\%$, in comparison to the co-NBI case.

To further study the suppression mechanism of ELMs by periodically alternating the direction of Neutral Beam Injection, the profiles of electron density n_e, electron temperature T_e and Doppler shift $f_{Doppler}$ from the Doppler Backscattering System (DBS) for the co-NBI and ctr-NBI H mode plasmas have been examined, as shown in Figure 2. Note that to minimize the collisionality effect on ELM, both of the line-averaged density n_e and diamagnetic energy W_E should be kept the same during the whole H-mode discharge, while

the co-NBI and ctr-NBI are alternated with each other. The density profiles in Figure 2 (a) were measured by the Low-Field-Side (LFS) reflectometry[13]. The electron temperature profiles were measured by edge multi-energy soft x-ray diagnostics, however the data at the edge ($R = 2.28 - 2.32m$) is not reliable (not shown)[14]. Here, the separatrix is located at $R = 2.32m$. The blue curve is the temperature profile at lower NBI heating power with $P_{co-NBI} = 0.2MW$. The profiles show that both density and temperature can be kept almost the same and consistent with the evolution of line averaged density and stored energy, which remain almost the same while the direction of NBI is periodically altered, as shown in Figure 1 (b). The normalized collisionality on the top of the pedestal is $\nu^* = 2.3$. Here, $n_{e,ped} = 3.5 \times 10^{19} m^{-3}$ and $T_{e,ped} = 300eV$. Comparing to the previous set-up in BOUT++ simulations in Ref. [15], the collisionality on EAST is much higher than the $n_0 = 5 \sim 9 \times 10^{19} m^{-3}$ cases with $\nu^* = 0.2 \sim 0.8$, but close to the $n_0 = 20 \times 10^{19} m^{-3}$ case with $\nu^* \simeq 6.19$. This suggests that EAST discharges are performed at high collisionality and ELMs on EAST are dominated by ballooning modes.

Figure 2 (c) illustrates the profiles of Doppler frequency $f_{Doppler}$ measured from the Doppler Backscatter System (DBS) on EAST, here the radial electric field E_r is proportional to $f_{Doppler}$ for $E_r = -B * u_\perp = -\frac{2\pi B}{k_\perp} f_D \propto f_{Dopper}$ with a fixed launch angle of DBS. It can be found that the Doppler frequency $f_{Doppler}$ wells in the pedestal region show big differences upon periodically altering the direction of NBI. The well becomes more negative at ctr-NBI case. The maximum value of $|E_r|$ $6.2kV/m$ at the bottom of E_r well. As shown in Figure 1 (f), the toroidal rotation changed from $\sim 50km/s$ to $\sim -10km/s$ after counter neutral beam injection, which contributed the negative radial electric field in the ion force balance equation ($E_r = \frac{1}{Z_i e n_i} \frac{\partial P_i}{\partial r} - V_{i\theta} B_\phi + V_\phi B_\theta$). Here, the V_ϕ is the velocity of toroidal rotation. The ELMs are suppressed by $\sim 80\%$ at ctr-NBI case with the maximal $|E_r|$ increased by a factor of ~ 2.7. Because we lack the detail toroidal and poloidal rotation profiles on the edge. It is not clear whether the change in the edge profile measured with Doppler reflectometry is due to the influence of the toroidal rotation at the edge or due to ion losses [16, 17]. The ion losses might play a significant role, which is also indicated by $20 - 30\%$ higher heating power necessary in the ctr-NBI phases to keep the stored energy W_E constant, as shown in Figure 1 (b) and (d).

Figure 3 shows the pedestal turbulence study with co- and ctr- NBI. Here, the temperature fluctuations $\tilde{T}_e$ are measured by the Electron Cyclotron Emission Radiometry (ECE) at

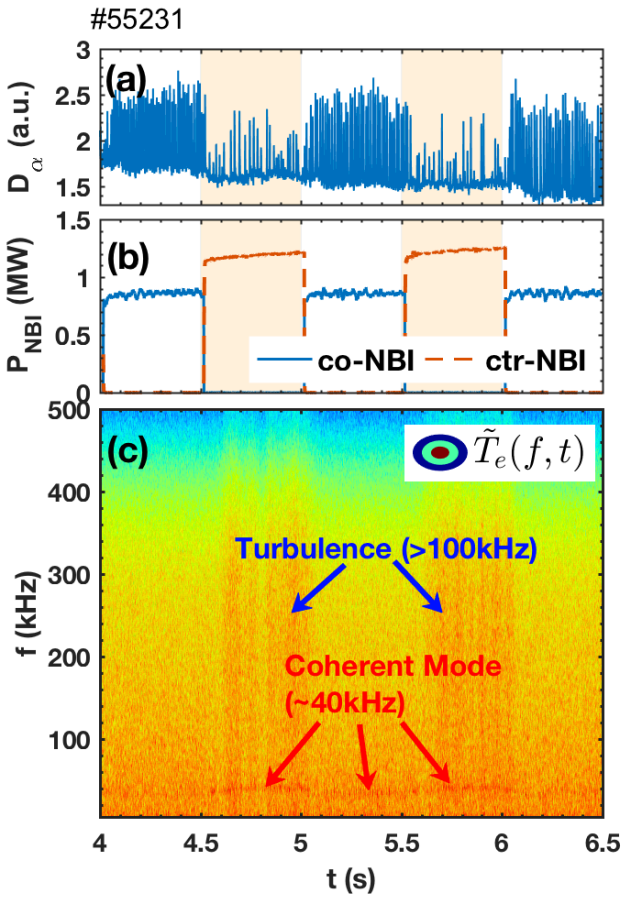

FIG. 3: Time evolutions of (a) D_α signal, (b) co- and ctr-current NBI power P_{NBI}, (c) spectrum of temperature fluctuations $\tilde{T}_e$ from ECE system

$r-a \sim -2cm$, which is close to the top half of the pedestal [18]. The bandwidth of the ECE system is around $400kHz$. It is shown in Figure 3 (a) that the ELM size is greatly suppressed at the onset of ctr-NBI. At the same time, the power of the pedestal turbulence increases dramatically, especially for high frequency turbulence with $f > 100kHz$. That is also found from the auto-power spectrum of $\tilde{T}_e$ as shown in Figure 4 (a). As $E \times B$ flow increased in the ctr-NBI case (Figure 2 (c)), the peak of the spectrum shifts to higher frequency, e.g. the frequency of the coherent mode changed from $\sim 32kHz$ to $\sim 42kHz$, as shown in Figure 3 (b). It is unfortunate that we lack the effective measurement of the abnormal particle flux on EAST during the H-mode discharge. Yet, considering the evolutions of the divertor ion flux, we can find that the particle transport contributed by the wide broadband mode ($> 20kHz$) in ctr-NBI discharge is not large enough when comparing the particle transport contributed by ELM.

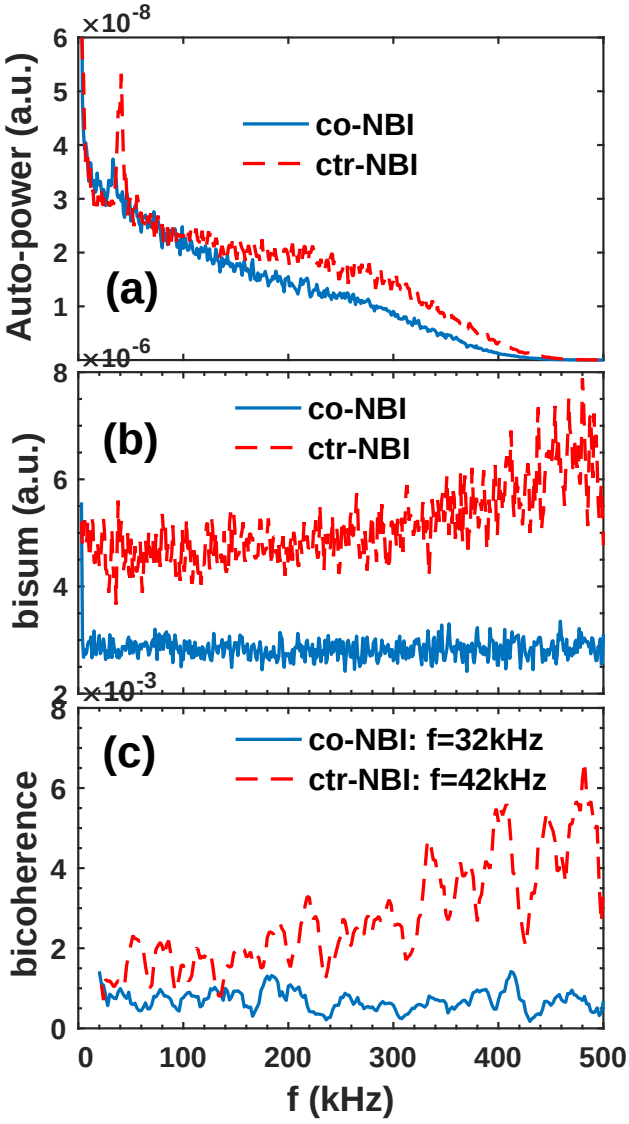

FIG. 4: (a) Auto-power spectrum of $\tilde{T}_e$, (b) summed squared bicoherence of $\tilde{T}_e$ and (c) bicoherence spectra of the coherent mode in co-NBI and ctr-NBI discharge, respectively.

The impact of nonlinear interaction on the ELM crash has been studied in Ref.[5, 19, 20]. The results indicate that the occurrence and characteristics of the crash depends on both the linear mode growth rate $\gamma(n)$ and the phase coherence time (PCT, $\tau_c(n)$), which is defined as the time duration of the relative cross phase $\delta\Phi$ between potential $\tilde{\phi}$ and pressure $\tilde{P}$ fluctuations and is set by nonlinear mode interaction. The relative phase between the potential and pressure perturbations is defined as: $\delta\Phi_{\tilde{P}\tilde{\phi}}(n,\psi,\theta,t) = \arg[\tilde{P}_n(\psi,\theta,t)/\tilde{\phi}_n(\psi,\theta,t)], \delta\Phi \in (-\pi,\pi]$, in which the $\tilde{P}_n$ and $\tilde{\phi}_n$ are the nth toroidal Fourier components of the pressure and potential perturbation, respectively. The relative phase is important because it deter-

mines whether the ballooning mode can extract free energy from the pressure gradient or not. The curvature term drives ballooning modes when $0 < \delta\phi < \pi$ (phase for growth) and damps ballooning mode when $-\pi < \delta\phi < 0$ (phase for damping). Thus, the net increase in amplitude due to linear drive is set by $\gamma(n)\tau_c(n)$, where the phase coherence time (PCT) $\tau_c(n)$ is defined as the time duration of the phase for growth and is limited by nonlinear mode interaction.

Thus, it is worth to compare the nonlinear interactions of the pedestal turbulence for different $E\times B$ shears on EAST. The bispectrum of the $\tilde{T}_e$ has also been estimated, computed with a resolution of $1kHz$ and ensemble averaging 400 realizations, as illustrated in Figure 3 (e). The summed squared bicoherence (bisum) is applied to evaluate the intensity of nonlinear interaction between different modes with $\sum b^2(m) = \frac{1}{N}\sum_{m=k+l} b^2(k,l)$ [21]. Here, $b^2(k,l) = \frac{|<X_k X_l X^*_{k+l}>|^2}{<|X_k X_l|^2><|X_m|^2>}$. Figure 3 (e) shows that nonlinear interactions between modes with different frequencies exhibit great differences. With ctr-NBI, the increased $E\times B$ shear will significantly enhance the nonlinear interactions for the whole bispectrum, especially for the modes with $f > 300kHz$. The bicoherence of the coherent mode in the co-NBI case ($f = 32kHz$) and ctr-NBI case ($f = 42kHz$) are illustrated in the Figure 4 (c). The results show the similar trend shown in bisum spectrum that during ctr-NBI discharge (increased $E_r\times B$ shear) can enhance nonlinear interaction between the coherent mode and other modes with different frequencies. Although the ambient turbulence with $1kHz < f < 100kHz$ are almost the same for both co-NBI and ctr-NBI cases (Figure 3 (d)), the bisum $\sum b^2$ increases from $\sim 2.8\times 10^{-3}$ to $\sim 4.8\times 10^{-3}$, which is large compared to the statistical uncertainty 2.5×10^{-3} ($\simeq M^{-1}$, where $M = 400$ is the number of realizations). It is hard to distinguish the role of the coherent mode ($32 \sim 42kHz$) and the high frequency turbulence ($> 100kHz$) in ELM relaxtion, yet, the bispectrum analysis in Figure 3 (b) reveals that the nonlinear interactions increase in ctr-NBI (increased $E_r \times B$ shear) for both the coherent mode and high frequency turbulence. The results indicate that both coherent mode and high frequency turbulence can help to relax the phase coherence time of peeling ballooning mode (PBM), thus the size of ELM.

Here, simulations are conducted using a simple three-field two-fluid model, which is extracted from a complete set of BOUT two-fluid equations with the additional effect of hyper resistivity [22] [23] [24] [25]. The model consists of a minimum set of nonlinear equations for perturbations of the magnetic flux $A_{||}$, electric potential ϕ, and pressure P, which has

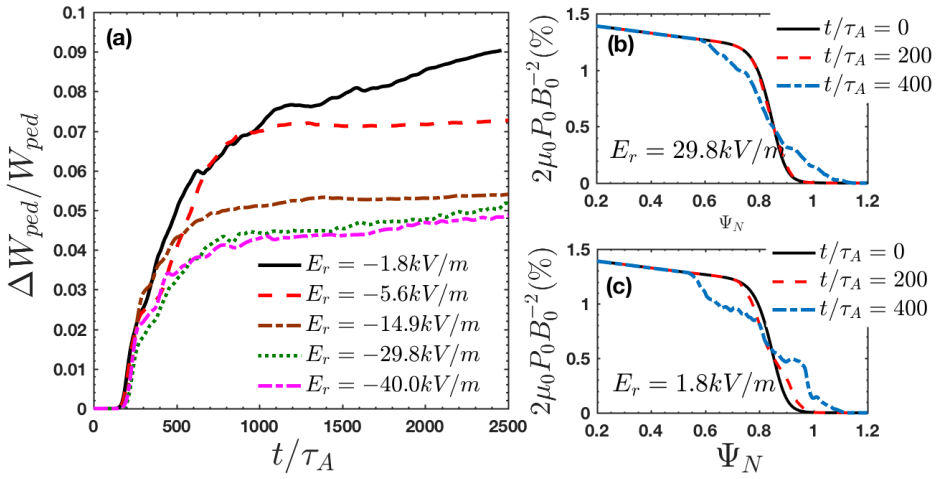

FIG. 5: (a) The time history of the plasma ELM loss fraction ($\Delta W_{ped}/W_{ped}$) of case $n_0 = 20 \times 10^{19} m^{-3}$ (high collisionality) for $E \times B$ scan. Radial total pressure profiles for cases with $E_r = -29.8kV/m$ (b) and $E_r = -1.8kV/m$ (c) at $t = 0\tau_A$ (black), $t = 200\tau_A$ (red), $t = 400\tau_A$ (blue), in which the Alfven time τ_A is $3.4 \times 10^{-7} s$.

been described in detail in Ref. [15]. The non-ideal physics effects include diamagnetic drift, $E \times B$ drift for typical pedestal plasmas.

To study the physics of nonlinear ELM dynamics, shifted circular cross-section toroidal equilibrium (cbm18-dens6) with fixed pressure gradient near the marginal P-B instability threshold has been used in our simulation[25]. Here, we examine five cases with different initial electric field profiles before the ELM, e.g. with $E_r = -1.8kV/m$, $E_r = -5.6kV/m$, $E_r = -14.9kV/m$, $E_r = -29.8kV/m$ and $E_r = -40kV/m$for $n_0 = 20 \times 10^{19} m^{-3}$, respectively. During the ELM phase, E_r changes with the pressure gradient due to the diamagnetic term, $E_r = E_{r0} + \frac{1}{(n_0 \cdot Z_i * e)} \cdot \nabla_r \cdot < p_i >$, where $< p_i >$ is the toroidal averaged pressure fluctuation. The neo-classical collisionality ν^* at the peak gradient is fixed at 6.18 for these five cases. Thus, the pedestal fluctuation is dominanted by the ballooning mode [26–29]. We reproduce the equilibrium with toroidal equilibrium module (TEQ) in CORSICA code [30], while keeping fixed the plasma cross-sectional shape, total stored energy, total plasma current, pressure, the radial location of the top of the pedestal density and temperature, the ratio of the density gradient scale length to the temperature scale length profiles. The detailed simulation setup is described in. Ref. [15].

To investigate how the ELM energy loss scales with $E \times B$ shear, the difference be-

tween the pre-ELM and post-ELM pressure profiles can be integrated to determine the energy lost at an ELM. We define an ELM size or ELM loss fraction as $\Delta_{ELM} = \Delta W_{PED}/W_{PED} = \langle \int_{\psi_{in}}^{\psi_{out}} d\psi \oint J d\theta d\zeta (P_0 - \langle P \rangle_\zeta) \rangle_t / \int_{\psi_{in}}^{\psi_{out}} P_0 d\psi \oint J d\theta d\zeta$, the ratio of the ELM energy loss (ΔW_{PED}) to the pedestal stored energy W_{ped}. The ELM size can be calculated from each nonlinear simulation. Here, P_0 is the pre-ELM pedestal pressure, P is the pedestal pressure during an ELM event, and symbol $\langle \rangle_\zeta$ means the average over the bi-normal periodic coordinate. The lower integral limit is the pedestal inner radial boundary $\psi_{in} = 0.1$, while the upper limit is the pivot point ψ_{out} (the radial position of the peak pressure gradient), J is the Jacobian.

Figure 5 (a) illustrates the time trace of the ELM energy loss fraction Δ_{ELM} evolution for the $E \times B$ shear scan. The signals show that if the ELM size keeps increasing, the pedestal collapse does not stop during the simulation period. When the pedestal crash occurs, filaments are generated and then evolve into turbulence. Here the definition of a filament is a helical coherent structure which moves radially outward. From the comparison of both ELM size (Figure 5 (a)) for the $E \times B$ shear scan in the high collisionality case and the radial total pressure profiles (Figure 5 (b) (c)) at $t = 0\tau_A$ (black), $t = 200\tau_A$ (red), $t = 400\tau_A$ (blue), it is manifest that the $E \times B$ shear can significantly suppress the ELM size and lead to a smaller crash and change on ∇P. The ELM energy loss is consistent with radial pressure profile crash.

Previous BOUT++ simulations in Ref. [5] show that the existence of linear instability alone does not predict ELM crashes. To trigger an ELM crash, the P-B perturbation must grow to a large, nonlinear amplitude. Linear drive and nonlinear wave-wave interaction both contribute to the growth of a mode. The nonlinear mode coupling will perturb the linear growth of the Peeling-Ballooning mode and significantly shorten its phase coherent time PCT τ_c. Theory suggests that ELMs can be controlled by either changing the growth rate spectrum or by shortening the phase coherence time.The growth rate of different modes is also extracted from linear growth stage ($0 \sim 200\tau_c$) of the nonlinear simulations, as shown in Figure 6 (b). Figure 6 (a) clearly shows that the ELM is significantly suppressed by increased $E \times B$ shear. $E \times B$ shear also reduces the growth rate, as shown in Figure 6 (b).

Figure 6 (c) illustrates the maximum phase coherence time $\tau_{c,max}(n)$ for each toroidal mode number for five different $E \times B$ shear cases mentioned above. Here, the $\tau_{c,max}(n)$ is longest duration of the relative cross phase $\delta\Phi$ between $\tilde{\phi}$ and $\tilde{P}$ with $0 < \delta\Phi < -\pi$. Because

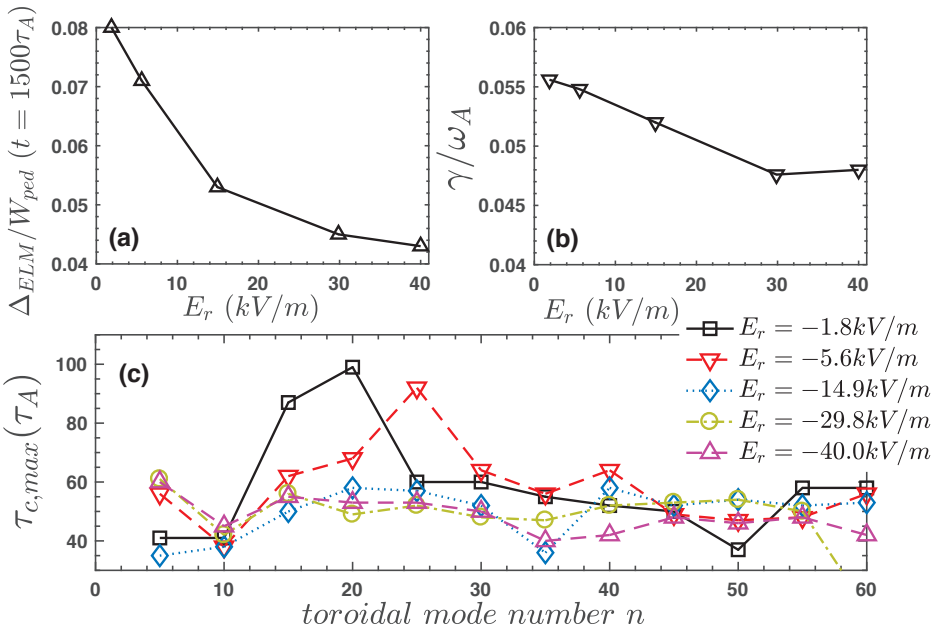

FIG. 6: . Nonlinear simulation results for an $E \times B$ shear scan at high collisionality ($n_0 = 20 \times 10^{19} m^{-3}$) (a) ELM size for different $E \times B$ shear at $1500\tau_A$; (b) linear growth rate; (c) the maximum phase coherence time for different toroidal mode number for cases with $E_r = -1.8kV/m$, $-5.6kV/m$, $-14.9kV/m$, $-29.8kV/m$ and $-40.0kV/m$, respectively.

of the exponential growth of the modes, $\tau_{c,max}$ is used to describe the largest amplitude achieved by a mode. The impact of $E \times B$ on $\tau_{c,max}$ is complex. As the electric field changed from $-1.8kV/m$ to $-14.9kV/m$, the peak $\tau_{c,max}$ shifts to higher n as shown in Figure 6 (c). The increased $E \times B$ shear significantly reduces the maximum τ_A of the intermediate-n modes with $15 \leq n \leq 25$. Figure 6 (c) shows that the larger $E \times B$ shear shortens the phase coherence time. In other words, the $E \times B$ decreased the phase coherence time and the growth rate, so the instabilities don't trigger the larger ELM. These results are consistent with the theory prediction and suggests that we can mitigated ELMs by increasing the $E \times B$ shear in high collisionality regimes.

In conclusion, by periodically alternating co-NBI and ctr-NBI at high collisionality in EAST, our studies show that both amplitude and frequency of ELMs can be modulated in a way consistent with simulation results. With the collisionality on the top of pedestal fixed at $\nu^* = 2.3$ (ballooning dominant case), counter injection of NBI greatly enhances the negative E_r well, while at the same time the ELM sizes are significantly reduced. The increased $E \times B$ can significantly enhance the amplitude of the pedestal turbulence at high

frequency, especially, modes with $f > 100kHz$. The nonlinear interactions between different modes have also been studied. The bispectrum for co-NBI and ctr-NBI cases indicate that increased $E \times B$ shear can enhance the nonlinear mode coupling of the pedestal turbulence. This inhibits the growth of ballooning modes, and supports the prediction that increased $E \times B$ can shorten the phase coherence time of the ballooning mode. . The simple three-field two-fluid model is applied to simulate the pedestal collapse and the ELM energy loss scaling with $E \times B$ shear in a fixed high collisionality regime with $\nu^* = 6.18$. The ELM size can be reduced by increased $E \times B$ shear due to the reduction of phase coherence time and linear growth rate, with both of which greatly affecting the amplitude of the ELM. Our study reveals that the increased $E \times B$ will shift the peak of phase coherent time to higher n (smaller scale turbulence). Those simulations suggest that ELMs can be mitigated by increasing $E \times B$ shear at high collisionality . The impact of $E \times B$ shear on ELMs at low collisionality warrants further study of simulations and experiments.

The authors thank the BOUT++ Team for support of these simulations, Lyu Bo, Guosheng Xu, Zhibin Guo, Adi Liu, Tianyang Xia, Yong Liu and Mickey Wade for the helpful comments. This work was performed under the auspices of the U.S. DOE by LLNL under Contract No. DE-AC52-7NA27344 and is supported by the International Partnership Program of Chinese Academy of Sciences No. Y16YZ17271, the Major / Innovative Program of Development Foundation of Hefei Center for Physical Science and Technology No.2018CXFX010, the China National Fusion Project for ITER under No.2014GB106003, and U.S. DOE under Award No. DE-FG02-04ERS4738.

[1] P. A. STURROCK. Model of the high-energy phase of solar flares. *Nature*, 211:695 EP –, 08 1966.

[2] K. Kusano, T. Maeshiro, T. Yokoyama, and T. Sakurai. The trigger mechanism of solar flares in a coronal arcade with reversed magnetic shear. *The Astrophysical Journal*, 610(1):537, 2004.

[3] Z. B. Guo and P. H. Diamond. From phase locking to phase slips: A mechanism for a quiescent h mode. *Phys. Rev. Lett.*, 114:145002, Apr 2015.

[4] J. G. Chen, X. Q. Xu, C. H. Ma, P. W. Xi, D. F. Kong, and Y. A. Lei. Impact of e b shear

flow on low-n mhd instabilities. *Physics of Plasmas*, 24(5):050704, 2017.

[5] P. W. Xi, X. Q. Xu, and P. H. Diamond. Phase dynamics criterion for fast relaxation of high-confinement-mode plasmas. *Phys. Rev. Lett.*, 112:085001, Feb 2014.

[6] Xi Chen, K.H. Burrell, N.M. Ferraro, T.H. Osborne, M.E. Austin, A.M. Garofalo, R.J. Groebner, G.J. Kramer, N.C. Luhmann Jr, G.R. McKee, C.M. Muscatello, R. Nazikian, X. Ren, P.B. Snyder, W.M. Solomon, B.J. Tobias, and Z. Yan. Rotational shear effects on edge harmonic oscillations in diii-d quiescent h-mode discharges. *Nuclear Fusion*, 56(7):076011, 2016.

[7] N. Oyama, Y. Sakamoto, A. Isayama, M. Takechi, P. Gohil, L.L. Lao, P.B. Snyder, T. Fujita, S. Ide, Y. Kamada, Y. Miura, T. Oikawa, T. Suzuki, H. Takenaga, K. Toi, and the JT-60 Team. Energy loss for grassy elms and effects of plasma rotation on the elm characteristics in jt-60u. *Nuclear Fusion*, 45(8):871, 2005.

[8] Y Sakamoto, H Shirai, T Fujita, S Ide, T Takizuka, N Oyama, and Y Kamada. Impact of toroidal rotation on elm behaviour in the h-mode on jt-60u. *Plasma Physics and Controlled Fusion*, 46(5A):A299, 2004.

[9] N. Aiba, M. Furukawa, M. Hirota, and S. Tokuda. Destabilization mechanism of edge localized mhd mode by a toroidal rotation in tokamaks. *Nuclear Fusion*, 50(4):045002, 2010.

[10] N. Aiba, M. Furukawa, M. Hirota, N. Oyama, A. Kojima, S. Tokuda, and M. Yagi. Mechanisms of plasma rotation effects on the stability of type-i edge-localized mode in tokamaks. *Nuclear Fusion*, 51(7):073012, 2011.

[11] F. Orain, M. Bécoulet, G. T. A. Huijsmans, G. Dif-Pradalier, M. Hoelzl, J. Morales, X. Garbet, E. Nardon, S. Pamela, C. Passeron, G. Latu, A. Fil, and P. Cahyna. Resistive reduced mhd modeling of multi-edge-localized-mode cycles in tokamak x-point plasmas. *Phys. Rev. Lett.*, 114:035001, Jan 2015.

[12] S Pamela, G Huysmans, and S Benkadda. Influence of poloidal equilibrium rotation in mhd simulations of edge-localized modes. *Plasma Physics and Controlled Fusion*, 52(7):075006, 2010.

[13] Y.M. Wang, X. Gao, B.L. Ling, S.B. Zhang, T. Zhang, X. Han, S.C. Liu, Z.X. Liu, Y. Liu, and A. Ti. Development of the w-band density profile and fluctuation reflectometer on {EAST}. *Fusion Engineering and Design*, 88(11):2950 – 2955, 2013.

[14] Y. L. Li, G. S. Xu, K. Tritz, Y. B. Zhu, B. N. Wan, H. Lan, Y. L. Liu, J. Wei, W. Zhang, G. H. Hu, H. Q. Wang, Y. M. Duan, J. L. Zhao, L. Wang, S. C. Liu, Y. Ye, J. Li, X. Lin, and

X. L. Li. Edge multi-energy soft x-ray diagnostic in experimental advanced superconducting tokamak. *Review of Scientific Instruments*, 86(12), 2015.

[15] X. Q. Xu, J. F. Ma, and G. Q. Li. Impact of the pedestal plasma density on dynamics of edge localized mode crashes and energy loss scaling. *Physics of Plasmas*, 21(12):120704, 2014.

[16] A. Kirk, D. Dunai, M. Dunne, G. Huijsmans, S. Pamela, M. Becoulet, J.R. Harrison, J. Hillesheim, C. Roach, and S. Saarelma. Recent progress in understanding the processes underlying the triggering of and energy loss associated with type i elms. *Nuclear Fusion*, 54(11):114012, 2014.

[17] M Cavedon, T Ptterich, E Viezzer, F M Laggner, A Burckhart, M Dunne, R Fischer, A Lebschy, F Mink, U Stroth, M Willensdorfer, E Wolfrum, and the ASDEX Upgrade Team. Pedestal and e r profile evolution during an edge localized mode cycle at asdex upgrade. *Plasma Physics and Controlled Fusion*, 59(10):105007, 2017.

[18] X. Han, X. Liu, Y. Liu, C. W. Domier, Jr. N. C. Luhmann, E. Z. Li, L. Q. Hu, and X. Gao. Design and characterization of a 32-channel heterodyne radiometer for electron cyclotron emission measurements on experimental advanced superconducting tokamak. *Review of Scientific Instruments*, 85(7):073506, 2014.

[19] P. W. Xi, X. Q. Xu, X. G. Wang, and T. Y. Xia. Influence of equilibrium shear flow on peeling-ballooning instability and edge localized mode crash. *Physics of Plasmas*, 19(9), 2012.

[20] G. Q. Li, X. Q. Xu, P. B. Snyder, A. D. Turnbull, T. Y. Xia, C. H. Ma, and P. W. Xi. Linear calculations of edge current driven kink modes with bout++ code. *Physics of Plasmas*, 21(10), 2014.

[21] Young C. Kim and Edward J. Powers. Digital bispectral analysis and its applications to nonlinear wave interactions. *IEEE. Transactions on Plasma Science*, PS-7(2):120–131, 1979.

[22] X. Q. Xu, P. W. Xi, A. Dimits, I. Joseph, M. V. Umansky, T. Y. Xia, B. Gui, S. S. Kim, G. Y. Park, T. Rhee, H. Jhang, P. H. Diamond, B. Dudson, and P. B. Snyder. Gyro-fluid and two-fluid theory and simulations of edge-localized-modesa). *Physics of Plasmas*, 20(5):–, 2013.

[23] T.Y. Xia, X.Q. Xu, and P.W. Xi. Six-field two-fluid simulations of peeling–ballooning modes using bout++. *Nuclear Fusion*, 53(7):073009, 2013.

[24] B.D. Dudson, M.V. Umansky, X.Q. Xu, P.B. Snyder, and H.R. Wilson. Bout++: A framework for parallel plasma fluid simulations. *Computer Physics Communications*, 180(9):1467 – 1480,

2009.

[25] X. Q. Xu, B. Dudson, P. B. Snyder, M. V. Umansky, and H. Wilson. Nonlinear simulations of peeling-ballooning modes with anomalous electron viscosity and their role in edge localized mode crashes. *Phys. Rev. Lett.*, 105:175005, Oct 2010.

[26] X. L. Zou. *24th IAEA FEC, San Diego, US*, (PD/P8-08), 2012.

[27] A Loarte, G Saibene, R Sartori, D Campbell, M Becoulet, L Horton, T Eich, A Herrmann, G Matthews, N Asakura, A Chankin, A Leonard, G Porter, G Federici, G Janeschitz, M Shimada, and M Sugihara. Characteristics of type i elm energy and particle losses in existing devices and their extrapolation to iter. *Plasma Physics and Controlled Fusion*, 45(9):1549, 2003.

[28] I. Nunes, G.D. Conway, A. Loarte, M. Manso, F. Serra, W. Suttrop, the CFN, and ASDEX Upgrade teams. Characterization of the density profile collapse of type i elms in asdex upgrade with high temporal and spatial resolution reflectometry. *Nuclear Fusion*, 44(8):883, 2004.

[29] A. W. Leonard. Edge-localized-modes in tokamaksa). *Physics of Plasmas*, 21(9):–, 2014.

[30] James A Crotinger, L LoDestro, L Don Pearlstein, A Tarditi, TA Casper, and E Bickford Hooper. Corsica: A comprehensive simulation of toroidal magnetic-fusion devices. final report to the ldrd program. Technical report, Lawrence Livermore National Lab., CA (United States), 1997.